Advances in Geo-Energy Research

Vol. 18, No. 1, p. 7-20, 2025

Original article

Heterogeneity and anisotropy of tight conglomerates: Mechanisms and implications

Bo Zhou[1,2], Shuheng Du[3,4]*, Yun Wei[2], Zhuoshen Zong[3,4], Xinguo Duan[1]*, Yizhe Wang[5]

[1]*College of Energy Resources, Chengdu University of Technology, Chengdu 610059, P. R. China*

[2]*Research Institute of Exploration and Development, PetroChina Xinjiang Oilfield Company, Karamay 834000, P. R. China*

[3]*State Key Laboratory of Nonlinear Mechanics, Institute of Mechanics, Chinese Academy of Sciences, Beijing 100190, P. R. China*

[4]*School of Engineering Science, University of Chinese Academy of Sciences, Beijing 100049, P. R. China*

[5]*Department of Earth and Atmospheric Sciences, University of Alberta, Edmonton T6G2E3, Canada*

Keywords:
Macro-lens infrared thermal imaging
umbrella deconstruction
heterogeneity
anisotropy

Cited as:
Zhou, B., Du, S., Wei, Y., Zong, Z., Duan, X., Wang, Y. Heterogeneity and anisotropy of tight conglomerates: Mechanisms and implications. Advances in Geo-Energy Research, 2025, 18(1): 7-20.
https://doi.org/10.46690/ager.2025.10.02

Abstract:
Tight conglomerate reservoirs pose challenges to development due to their strong heterogeneity and anisotropy, while existing characterization technologies have limitations such as cumbersome sample preparation and low efficiency. Additionally, the microscale coupling mechanism among pores, elements, and components remains unclear. To address these issues, this study aims to reveal the controlling mechanisms of such reservoir features and establish an integrated characterization system. This system couples macro-lens infrared thermal imaging, umbrella deconstruction, field emission scanning electron microscopy, and energy dispersive spectroscopy, and adopts eight-directional physical slicing to systematically characterize the pores, elements, and components of tight conglomerate reservoirs. Results indicate that pores are more developed in specific directions. Characteristic elements exhibit distinct directional enrichment and depletion: Some elements reach high contents in certain directions, while others drop to very low levels. Mineral contents show angle-dependent variations; for example, the proportion of weakly weathered feldspar increases significantly with increasing angle. All these features are synergistically controlled by the original sedimentary fabric and late-stage diagenesis. This work enriches the microscopic characterization theory of tight reservoirs, provides microscopic evidence for identifying favorable reservoir zones, and offers direct technical support for optimizing wellbore deployment and avoiding high-risk fracturing areas in engineering practice.

1. Introduction

Tight conglomerate reservoirs are widely developed in large-scale lacustrine transgressive-regressive fan-delta sedimentary systems with well-developed fan-delta plains, fronts, and prodelta subfacies. Sand bodies here are widely distributed and interconnected, and tight conglomerate reservoirs mainly form in fan-delta plain channels, debris flows, and front subaqueous distributary channels. These reservoirs feature strong water sensitivity and heterogeneity. Cores disintegrate in fresh water and mostly even in formation water, which poses major challenges to utilization (Tan et al., 2017; Yu et al., 2022; Abitkazy et al., 2024; Zhai et al., 2025).

From a petrological perspective, the grain size of conglomerate is significantly larger than that of sandstone and shale (Qin et al., 2024; Wang et al., 2024a; Zhang et al., 2024; Chen et al., 2025), and this structural difference causes much higher reservoir complexity (Wang et al., 2022; Sun et al., 2023). This

Yandy Scientific Press

*Corresponding author.
E-mail address: zhbo-cq@petrochina.com.cn (B. Zhou); dushuheng@imech.ac.cn (S. Du); wy_xg@petrochina.com.cn (Y. Wei); zongzhuoshen20@mails.ucas.ac.cn (Z. Zong); duanxinguo888@hotmail.com (X. Duan); yizhewang99@yeah.net (Y. Wang).

Received August 1, 2025; revised August 26, 2025; accepted September 12, 2025; available online September 15, 2025.

complexity manifests in two key aspects: Heterogeneity and anisotropy (Guo et al., 2009; Sinan et al., 2020). Heterogeneity includes mineral composition heterogeneity and pore space heterogeneity; anisotropy refers to directional differences in reservoir properties including component distribution and mechanical properties, and directly affects engineering processes like hydraulic fracturing (Tan et al., 2023; Zhao and Du, 2024; Liu et al., 2025).

Tight conglomerate reservoirs are often polymodal with interspersed coarse and fine particles, which enhances their complexity. Despite abundant resources, the gap between resource potential and development efficiency remains notable, partly due to insufficient reservoir geological research. The current understanding of their heterogeneity and anisotropy is limited, as there is no comprehensive geological model. Efficient analysis of micro-scale, especially micro-nano scale, heterogeneity and anisotropy under large sample sizes is critical, as these features regulate core properties like permeability and fluid occurrence.

Existing technologies such as optical microscopy, scanning electron microscopy, and computed tomography scanning have achieved phased results but suffer from cumbersome sample preparation, low efficiency, and over-reliance on experience, failing to meet demands for rapid batch analysis of static and dynamic core samples (Kazak et al., 2021; Zhan et al., 2022; Wood, 2024). Frankly, existing studies on tight conglomerates have three key gaps. First, the coupling mechanism of micro-scale heterogeneity and anisotropy among pores, elements, and components remains unclear, especially the angle-dependent correlation between sedimentary fabric and diagenetic processes (Mokhtari et al., 2016). Second, traditional techniques cannot integrate efficient signal acquisition, multi-dimensional deconstruction, and quantitative characterization, failing to meet dynamic monitoring and batch analysis needs (Fjær and Nes, 2014; Sun et al., 2018). Third, the link between micro-scale features and macro-scale engineering is missing, limiting the application of micro-characterization results (Eaton, 2006; Fitch et al., 2015; Zoccarato et al., 2016).

The umbrella deconstruction method has been used to analyze reservoir microscopic structures and has broken through the limitations of the traditional "reservoir black box" (Du et al., 2018, 2019). Its core is slicing cores in 8 representative spatial directions and using scanning electron microscopy and polarizing microscopy to analyze microfeatures, improving characterization authenticity. However, early applications relied heavily on these two techniques, requiring conductive coatings that prevented dynamic observation and distorted post-fluid-contact testing (Zhang et al., 2018; Worden and Utley, 2022; Wang et al., 2024b). Additionally, testing was time-consuming, limiting batch processing and efficiency, so new technical paths are needed (Zimmermann et al., 2015; Khattak et al., 2024).

Infrared thermal imaging offers non-contact detection, real-time response, and large-range scanning, but its low spatial resolution restricts its microscopic use in reservoir analysis (Khanal et al., 2017; Hou et al., 2022). The present study introduces macro-lens infrared thermal imaging and couples it with umbrella deconstruction, scanning electron microscopy, and energy dispersive spectroscopy to establish an integrated system for microscopic thermal signal acquisition, multi-dimensional feature deconstruction, and quantitative characterization. This system uses macro-lens infrared imaging efficiency to compensate for the shortcomings of the other two techniques, enables dynamic observation, and solves coating-related bottlenecks.

Focused on tight conglomerate reservoirs, the study aims to establish quantitative indicators for mineral and pore heterogeneity based on thermal signal spatial differences and build a correlation model between the thermal response anisotropy and reservoir directional features to reveal anisotropy mechanisms. Ultimately, it seeks to enrich tight reservoir characterization theory, provide efficient microscopic analysis tools, and support tight conglomerate reservoir evaluation and optimization.

2. Methodology

All samples were collected from key formations of tight conglomerate reservoirs, ensuring strong correlation with the study's core objectives. During sample selection, pre-evaluation was conducted via core observation and conventional petrophysical tests to ensure selected samples' petrophysical parameters match the overall range of typical tight conglomerate reservoirs. The porosity of these samples ranges from 4.2% to 12.5% and permeability from 0.1 to 5.3×10^{-3} μm^2, with no significant deviations. Subsequent multi-technique characterization results of these samples are highly consistent with published geological backgrounds and reservoir characteristics of tight conglomerates, further verifying sample representativeness.

2.1 Scanning electron microscopy imaging

Field Emission-Scanning Electron Microscopy (FE-SEM) is widely used for microscopic characterization of tight reservoirs. It distinguishes granular minerals and pore-throat spaces by leveraging differences in electron signal responses between solid minerals and spaces (Camp et al., 2025) and operates with an electron beam acceleration voltage of 10 kV, a working distance of 10.8 mm, a maximum imaging magnification of 300,000×, an imaging resolution of 0.5-10 nm, and an observation scale of up to approximately 20 mm through imaging stitching. This technique balances high resolution and sample representativeness, overcoming the insufficient representativeness of Micro-CT and Nano-CT which stems from their small sample sizes and the limited observation range of Focused Ion Beam-Scanning Electron Microscopy (FIB-SEM). After imaging, data processing steps including image denoising, gray threshold segmentation, and pore-mineral unit extraction yield quantitative parameters such as porosity, pore-throat radius, pore solidity, pore fractal dimension, and mineral particle shape. These support the analysis of microscopic heterogeneity, anisotropy, and seepage capacity. Compared with Micro-CT that has low mineral identification accuracy relying on CT values and high testing costs, it is more convenient and economical, serving as a core technique for fine characterization of tight reservoir microstructures.

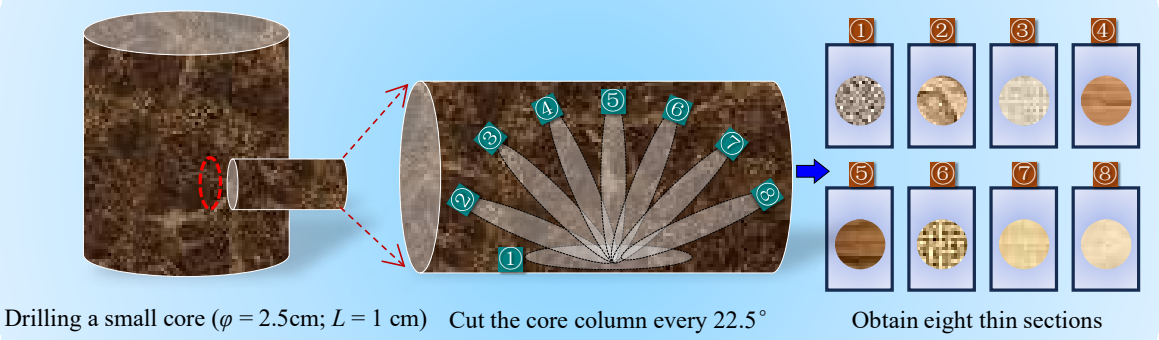

Fig. 1. Experimental concept of umbrella deconstruction (Revised after Du et al. (2019)).

Pore size and geometric parameters are calculated using the image processing software ImageJ: Gaussian filtering eliminates electronic noise interference at pore boundaries, Otsu's automatic thresholding method determines the threshold by maximizing the between-class variance of pores and minerals, and the Canny edge detection algorithm ensures complete pore contour extraction and pseudo-pore removal. After threshold optimization, the "analyze particles" module automatically extracts parameters including the ellipse-fitted major axis, ellipse-fitted minor axis, and Feret diameter. The major and minor axes refer to the lengths of the equivalent ellipse's long and short axes for each pore, the aspect ratio being their ratio, and the Feret diameter being the maximum and minimum distances across a pore along a specific direction. Circularity is defined as four times the pore area divided by the product of π and the square of the pore perimeter, with a value of 1 indicating a perfect circle and smaller values meaning greater deviation from a circle. Roundness lacks a universal formula and is often confused with circularity; some cases adopt a formula of four times the pore area divided by the product of π and the square of the ellipse-fitted major axis length to emphasize the major-minor axis ratio. Solidity is the ratio of the pore area to its convex hull area, with a value of 1 indicating a full shape without concavities and smaller values indicating more concavities.

2.2 Energy dispersive spectrometer testing

Energy Dispersive Spectrometer (EDS) testing is based on the principle of X-ray fluorescence spectroscopy for element analysis (Liu et al., 2022). When the sample surface is bombarded by a high-energy electron beam, the test usually coupled with FE-SEM, which provides the excitation source. This bombardment knocks out inner-shell electrons of atoms. The transition of outer-shell electrons to fill these vacancies releases characteristic X-rays that are unique to each element. The detector captures this signal and converts it through the energy spectrum analysis system. This process enables qualitative identification of elements and quantitative calculation of their relative content. The core of the method is to use the differences in energy and intensity of characteristic X-rays from different elements to establish a quantitative relationship between the element composition and distribution of the sample.

EDS testing and FE-SEM form a technical coupling for simultaneous morphology-composition characterization. FE-SEM provides microscopic morphology imaging of the sample to locate the analysis area. EDS then conducts element analysis on this specified area. This coupling avoids the limitation that single morphology observation cannot distinguish mineral composition. The sample analysis range can reach 5 mm $\times$ 5 mm. The analysis objects cover key elements of tight reservoirs, including oxygen, silicon, aluminum, potassium, calcium, magnesium, and iron. Mineral types can be distinguished through element content statistics. For example, calcite is identified based on calcium content distribution and potassium feldspar is identified based on potassium content. The anisotropy of element composition can also be quantified. In data processing, standardization correction and inter-direction comparison analysis of element content are required to eliminate test system errors. This ensures the accuracy of interpreting element distribution laws, geological processes such as compaction and dissolution, and reservoir properties such as brittleness and seepage capacity.

2.3 Umbrella deconstruction characterization

The umbrella deconstruction method relies on eight-directional umbrella-shaped physical slicing of rock samples, which overcomes the contradiction between resolution and observation scale of computed tomography. Through multi-technique coupling, it quantifies the two-dimensional distribution of pores, minerals, and fractures, reveals the genetic mechanisms of heterogeneity, provides evidence for sweet spot identification, and enhances sample representativeness (Fig. 1).

Its technical principle involves using a standard core drill string with a diameter of 25 mm and a length of 50 mm. Mark lines are set every 22.5° on the core end face to obtain 8 directional thin sections. Combined with FE-SEM and EDS, it realizes the unification of large-range observation and microscopic identification. It extracts pore, mineral, and element parameters to quantify heterogeneity and anisotropy, making up for the limitations of traditional technologies. Its development has shown a gradual expansion and deepening trend. Specifically, a heterogeneity evaluation system was built in 2018. By 2019, its application scope had expanded to element anisotropy and permeability prediction. In 2020, the significance of parameters was further deepened, which

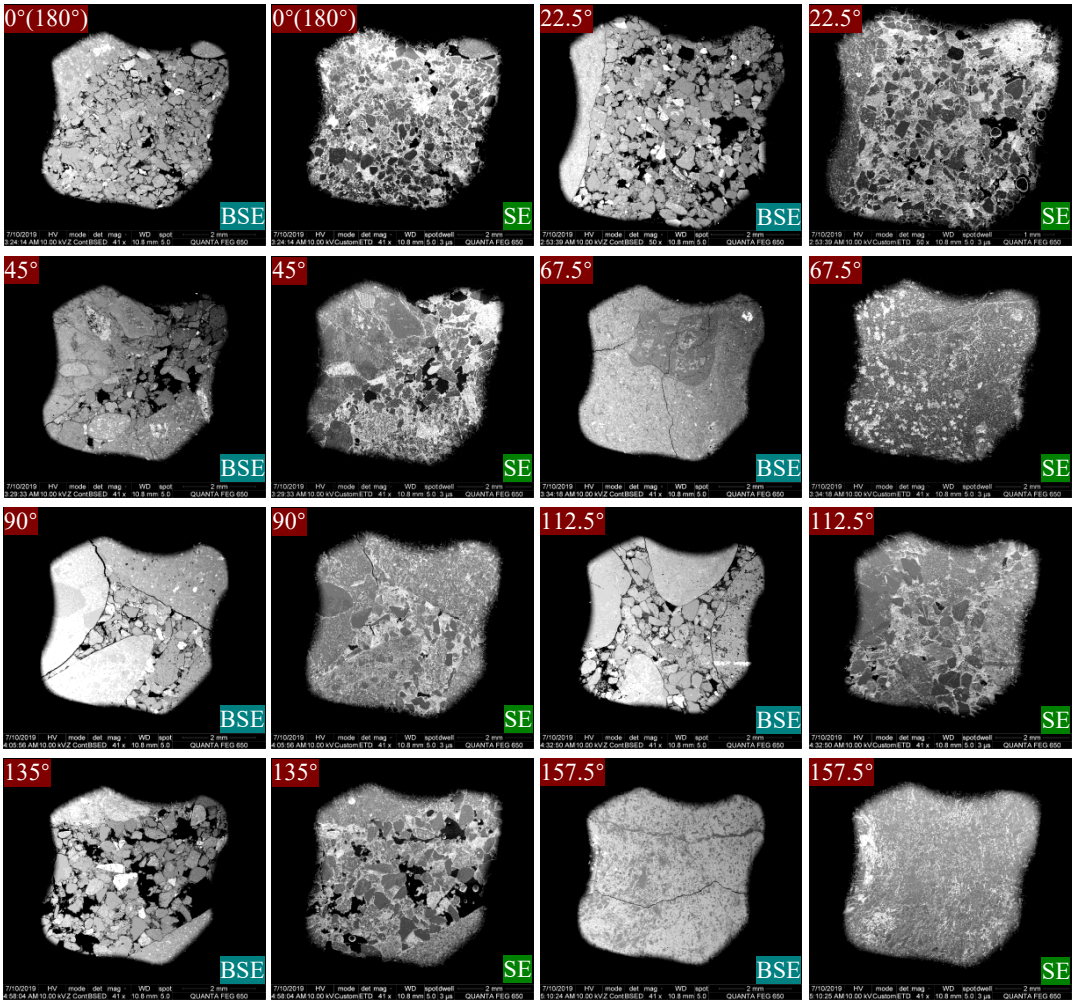

Fig. 2. Backscattered and secondary electron characterization results of 8 directional slices.

eventually led to the formation of a complete technical system (Du et al., 2018, 2019; Du, 2020).

2.4 Macro-lens infrared thermal imaging

The core principle of macro-lens infrared thermal imaging technology is based on Planck's blackbody radiation law (Du et al., 2025). Any object above absolute zero emits specific-wavelength infrared radiation, with its intensity and wavelength distribution varying with temperature and surface emissivity. By coupling a high-magnification macro lens to traditional systems, it shortens the imaging working distance, optimizes the optical focal length and detector sensitivity, and improves spatial resolution to the micron level. It has 640×480 infrared resolution and $1,280 \times 960$ via super-pixel technology, an uncooled infrared focal plane array detector, 30 mK thermal sensitivity, and a 17 μm pixel pitch, enabling accurate capture of thermal signals from reservoir samples.

This system uses an uncooled infrared focal plane array detector, featuring high response speed and low noise to record real-time thermal field changes of samples, meeting dynamic observation needs like water-rock interaction (Cha et al., 2012; Balatsenko, 2023; Molineux et al., 2024). Experiments use a constant temperature and humidity chamber and a 2-hour sample equilibration to avoid ambient interference. Samples need no conductive coating, preserving their original state and test authenticity. Infrared signals are output as grayscale images or temperature fields. Image analysis quantifies thermal radiation differences, which are correlated with reservoir mineral composition and pore distribution, providing thermophysical data for characterizing microscopic heterogeneity and anisotropy.

3. Results and Discussion

3.1 Pore heterogeneity and anisotropy

Scanning Electron Microscopy was used to simultaneously conduct backscattered electron (BSE) imaging and secondary electron (SE) imaging on 8 directional slices of the tight conglomerate reservoir. Fig. 2 presents the results of these characterizations. Combined with fine image processing technology, we obtained quantitative data covering pore size parameters and morphological parameters. A unified system for pore size parameters was adopted, including pore radius, pore perimeter, ellipse-fitted major axis, ellipse-fitted minor axis, maximum Feret diameter, and minimum Feret diameter. This system quantitatively describes pore geometric features from multiple

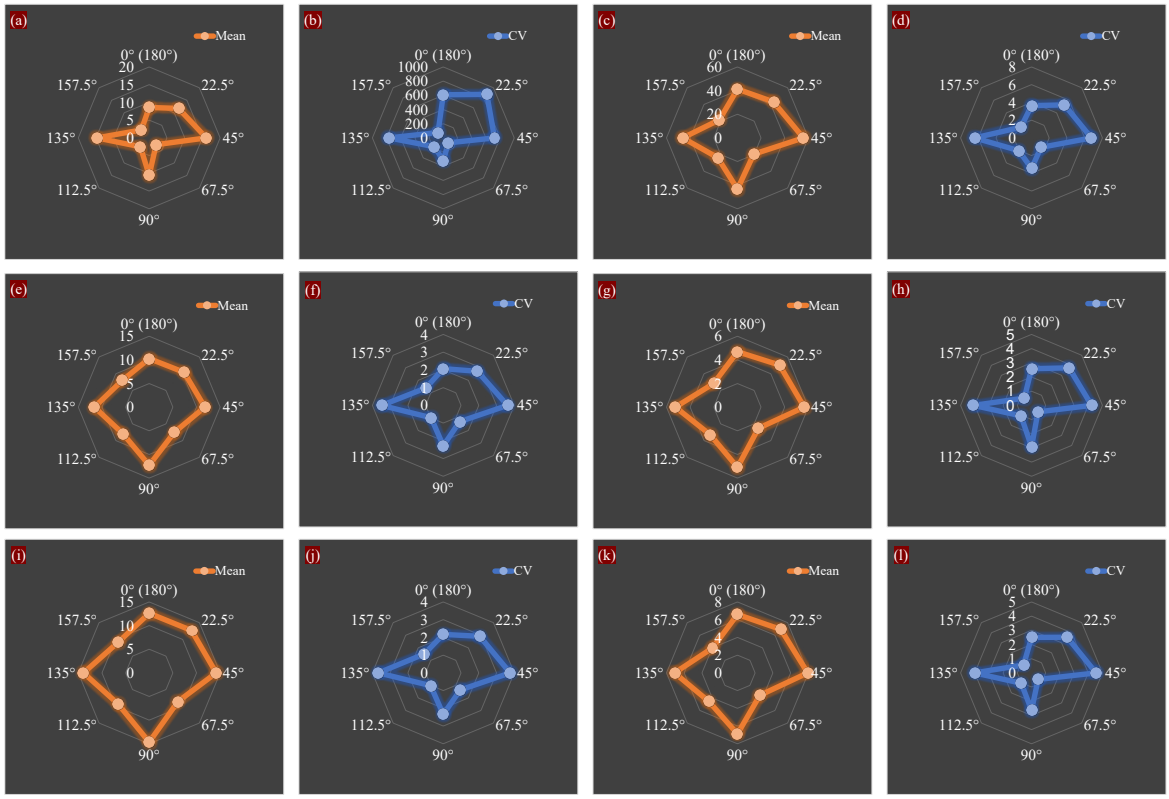

Fig. 3. Results of pore size parameter heterogeneity and anisotropy: (a), (c), (e), (g), (i) and (k) denote the distributions of mean values of radius, perimeter, major axis length, minor axis length, Feret diameter, and minFeret, respectively; while (b), (d), (f), (h), (j) and (l) correspond to the distributions of their coefficient of variation (CV) across the same eight directions. All parameter values are in units of micrometers.

dimensions, providing a consistent methodological basis for cross-directional comparison. Combined with the data analysis in Fig. 3, the ratio of maximum to minimum mean values and the ratio of maximum to minimum coefficient of variation of all pore size parameters across the 8 directions are significantly greater than 1. This indicates significant differences in pore size mean value and dispersion degree among directions, revealing obvious anisotropy in the reservoir pore system that reflects directional control of diagenesis or sedimentary fabric on pore development. Variation trends of ellipse-fitted axes and Feret diameters are highly synchronized, verifying the intrinsic correlation between pore long and short dimensions and confirming the consistency of different characterization methods for pore geometric shapes.

High-value regions of pore size parameters concentrate in middle-angle directions where pores are more developed, while low-value regions are in other specific directions. The coefficient of variation shows directional differentiation, with high values in some middle-angle directions indicating significant pore size differences and prominent inhomogeneity, and low values in other directions reflecting uniform pores. Extreme values of parameters mostly distribute in middle-angle directions as maximum values and specific other directions as minimum values, showing clear differentiation between dominant and disadvantaged pore development directions – a specific manifestation of pore size heterogeneity. Geologically, this anisotropy and directional dependence result from the combined effects of diagenesis and original sedimentary fabric, including uneven paleofluid dissolution in some directions and stronger particle compaction with denser cement filling in others. Engineering-wise, directions with high pore size values have large radii and long Feret diameters, leading to small fluid migration resistance and serving as dominant seepage directions. Directions with a high coefficient of variation show strong reservoir inhomogeneity and significant fluid flow anisotropy. In drilling and fracturing engineering, priority should be given to dominant seepage directions for wellbore deployment or fracture design to improve productivity, while preventing stress concentration and reservoir instability from strong pore size dispersion.

Pore morphological characteristics are characterized by ellipse aspect ratio, boundary shape factor (circularity), roundness, solidity, ellipse major axis extension angle, and maximum Feret diameter extension angle. A unified quantitative system was established from geometric shape, boundary feature, and directional extension dimensions to support analysis of pore morphology anisotropy, with relevant results shown in Fig. 4. Data show that the ratio of maximum to minimum mean values and the ratio of maximum to minimum coefficient of variation of all morphological parameters across the 8 directions are greater than 1, confirming significant directional differences in mean value and dispersion degree that reflect

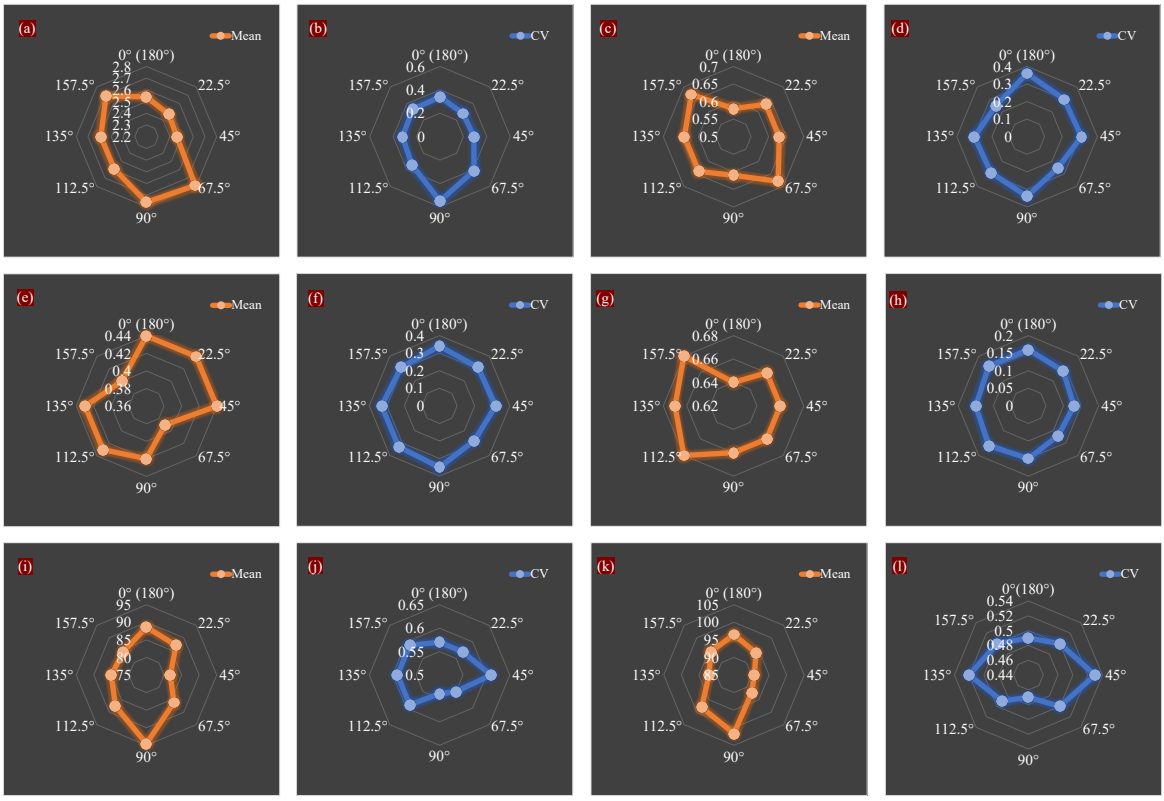

Fig. 4. Results of pore morphological parameter heterogeneity and anisotropy: (a), (c), (e), (g), (i) and (k) denote the distributions of mean values of aspect ratio, circularity, roundness, solidity, angle, and Feret angle across the eight directions, respectively; while (b), (d), (f), (h), (j) and (l) correspond to the distributions of their CV across the same eight directions. Except for the two parameters namely angle and Feret angle, whose units are degrees, all other parameter values are dimensionless.

directional control of diagenesis or sedimentary fabric on pore morphology. Variation trends of the two extension angles are coordinated, verifying intrinsic consistency of dominant pore extension directions. For ellipse aspect ratio, mean values vary directionally with higher values in some directions indicating flatter pores; the coefficient of variation differs with stronger dispersion in certain directions reflecting pore flatness differences. This arises from pore stretching in these directions due to diagenetic dissolution or particle arrangement, guiding fluid seepage with smaller resistance along the major axis. A higher coefficient of variation in other directions stems from dissolution inhomogeneity or particle contact differences, enhancing seepage anisotropy. For circularity, smaller values mean more tortuous boundaries. Mean values are lower in one direction for more tortuous boundaries and higher in others for smoother boundaries. The coefficient of variation is strong in some directions and weak in others. Lower values result from heterogeneous dissolution increasing seepage resistance, while higher values reflect regular diagenesis or original pores facilitating migration. For roundness, larger values indicate more circle-like shapes – mean values are lower in some directions for irregular pores and higher in others for rounder pores; the coefficient of variation is strongest in a specific direction. Lower values link to stretched non-circular pores, while higher values come from isotropic dissolution weakening seepage anisotropy. For solidity, larger values mean more convex pores. Mean values are lower in one direction for concave-convex pores and higher in others for fuller pores. The coefficient of variation is weakest in a specific direction. Lower values form seepage bottlenecks from heterogeneous dissolution or clay filling, while higher values ensure continuous seepage space via uniform cementation or compaction. For the two extension angles, the coefficient of variation is low in one direction, indicating a dominant extension direction tied to tectonic stress or gravel arrangement, serving as a fluid migration channel. A higher coefficient of variation in other directions reflects scattered extension from local particle boundaries or microfractures, providing guidance for horizontal well trajectory design and fracturing optimization.

Fig. 3 includes the distribution of mean values and coefficient of variation (CV) values of the reservoir's pore radius, pore perimeter, ellipse-fitted major axis, ellipse-fitted minor axis, maximum Feret diameter, and minimum Feret diameter across the eight directions. Fig. 4 includes the distribution of mean values and CV values of the reservoir's ellipse aspect ratio, boundary shape factor (circularity), roundness, solidity, ellipse major axis extension angle, and maximum Feret diameter extension angle across the eight directions.

3.2 Element heterogeneity and anisotropy

EDS was employed to determine elemental contents across the 8 directional slices of the tight conglomerate reservoir.

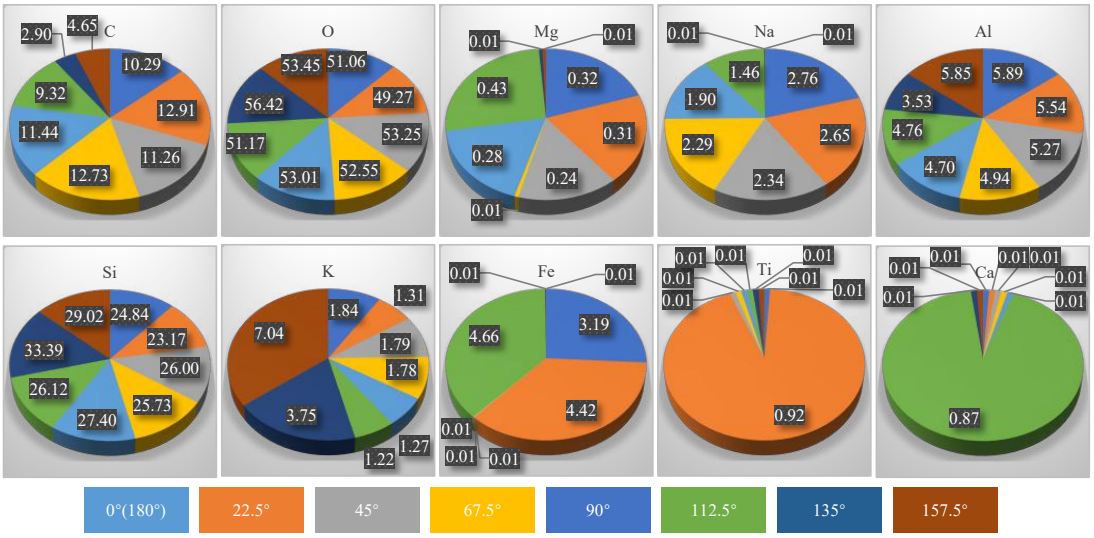

Fig. 5. Heterogeneity and anisotropy of element content ratio. (The sum of all element contents in the same sample may slightly deviate from 100%, mainly caused by system measurement errors.)

Fig. 5 presents the relevant results. Silicon and oxygen, core elements of siliceous minerals like quartz, exhibit generally high contents across all directions. Their mean contents are 26.96% for silicon and 52.52% for oxygen, forming the rock's main mineral framework. Aluminum, a characteristic element of aluminosilicates such as feldspar and clay minerals, shows relatively stable content with a mean of 5.06%, indicating the widespread presence of aluminosilicate minerals in the reservoir.

Beyond this baseline distribution, the heterogeneity and anisotropy of elemental parameters are prominent in three key aspects. First, characteristic elements display directional enrichment and depletion. Sodium reaches maximum content in one direction and minimum in other specific directions, with the latter showing nearly depleted sodium. Magnesium peaks in a certain direction and drops to minimal levels in other directions, also showing depletion in the latter. This is likely due to intense leaching of feldspar where fluids in dominant seepage channels carry away soluble cations, while directions with weaker leaching preserve more sodium and magnesium. Potassium is enriched in one direction and depleted in another, corresponding to the accumulation of potassium feldspar or potassium-rich clay minerals like illite. Iron peaks in two specific directions and is minimal in others, reflecting the directional distribution of iron oxides such as hematite or iron-bearing clays like chlorite, as well as differences in iron migration and accumulation in diagenetic fluids. Titanium concentrates locally in one direction, linked to accessory minerals like ilmenite and rutile, and is negligible in most other directions. Calcium enriches in a certain direction, corresponding to the directional distribution of calcite cement, and is also minimal elsewhere, indicating localized diagenetic activity of carbonate fluids. Second, carbon content fluctuates significantly across directions. It reaches high levels in one direction and falls to low levels in another, with a coefficient of variation of 0.37, which is higher than that of most major elements. High carbon content in one direction may result from organic matter enrichment or concentrated carbonate cementation, while carbon depletion in another direction stems from intense leaching or low organic matter input. This reflects directional differences in the sedimentary environment, such as organic matter input intensity, or diagenetic transformation like decarbonation. Third, elemental ratios respond directionally to diagenesis. The Si/Al ratio varies notably across directions, with a much higher ratio in one direction than another. A high Si/Al ratio indicates relative enrichment of siliceous materials such as quartz overgrowth and siliceous cement along with depletion of aluminous materials due to feldspar weathering. A low ratio suggests preserved aluminous components from limited feldspar weathering, revealing anisotropy in silico-aluminous diagenetic processes. The K/Na ratio shows extreme directional variation, being extremely high in one direction and less than 1 in another. This reflects differences in potassium metasomatism intensity or sodium leaching – one direction may have experienced strong potassium-bearing fluid activity or sodium leaching, while another retained more sodium with weaker potassium-related processes, indicating directional changes in diagenetic fluid chemistry.

Fig. 5 shows the heterogeneity and anisotropy of element content ratios. The heterogeneity and anisotropy of elemental parameters hold significant geological and engineering implications. Directional elemental differences directly mirror the anisotropy of diagenetic processes, including leaching, cementation, and metasomatism, and are tightly linked to paleofluid migration directions and original rock fabric, such as fluid channels controlled by gravel arrangement. For instance, directions with depleted sodium and magnesium likely correspond to dominant seepage channels where intense fluid activity removed soluble components. Conversely, directions with enriched potassium, iron, titanium, and calcium may be areas of directional diagenetic mineral precipitation. These variations lead to anisotropy in reservoir physical properties

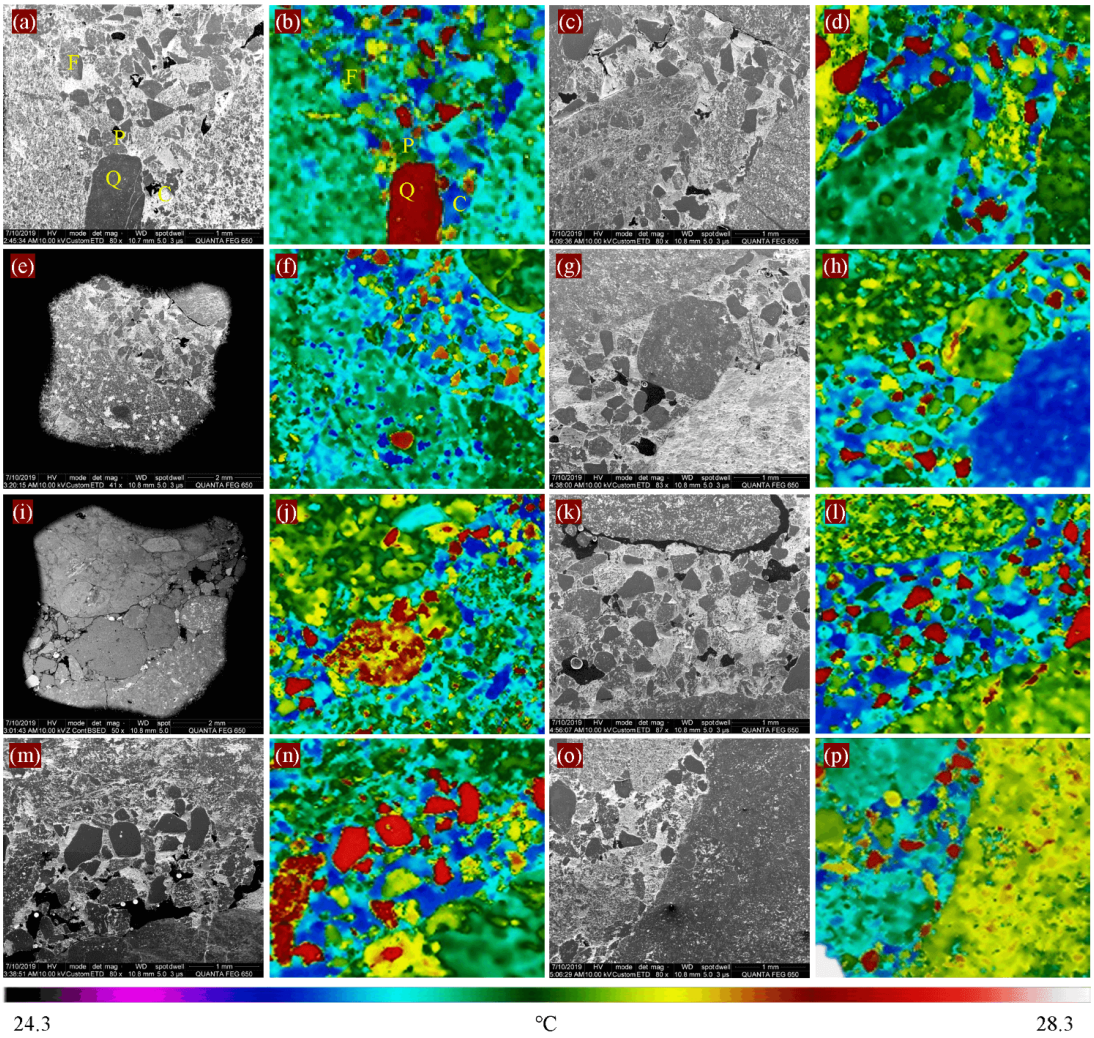

Fig. 6. Reservoir component interpretation based on macro thermal imaging: (a), (c), (e), (g), (i), (k), (m), (o) show the key electron microscope images, while (b), (d), (f), (h), (j), (l), (n), (p) show the corresponding thermal images for the same eight viewing directions.

like porosity and permeability due to differences in mineral filling or dissolution, providing a geochemical basis for reservoir evaluation and development, such as guiding horizontal well trajectory selection to target zones with favorable fluid flow characteristics.

3.3 Component heterogeneity and anisotropy

3.3.1 Component interpretation

Macro-lens infrared thermal imaging technology was used to test the apparent temperature of the 8-directional slices of the tight conglomerate reservoir, with emissivity uniformly set to 1. Fig. 6 shows the reservoir component interpretation based on macro thermal imaging.

By comparing the macro-lens infrared thermal images and secondary electron images in the same field of view (Fig. 6), we found that quartz, feldspar, illite-smectite mixed-layer clay, and pores in the secondary electron images can well correspond to different temperature ranges in the macro-lens infrared thermal images, as shown in Table 1. The differences in apparent temperature among different minerals come from inherent differences in their physical properties and microstructures. Quartz has a dense crystal structure and stable infrared radiation characteristics, so it has the highest temperature and small temperature difference. As feldspar weathering degree weakens, its crystal structure becomes more complete and thermal radiation capacity stronger, leading to higher temperature. However, structural damage from weathering slightly increases the temperature difference. Clay minerals exist as fine-grained dispersion, with a large specific surface area and rapid heat exchange. They quickly reach thermal equilibrium under external constant temperature, resulting in the lowest temperature and smallest temperature difference. The present study thus achieves the conversion of macro-lens infrared thermal images into reservoir component images. Macro-lens infrared thermal images can be acquired with very high efficiency on the order of seconds, while acquiring secondary electron images requires a relatively complex sample pretreatment process.

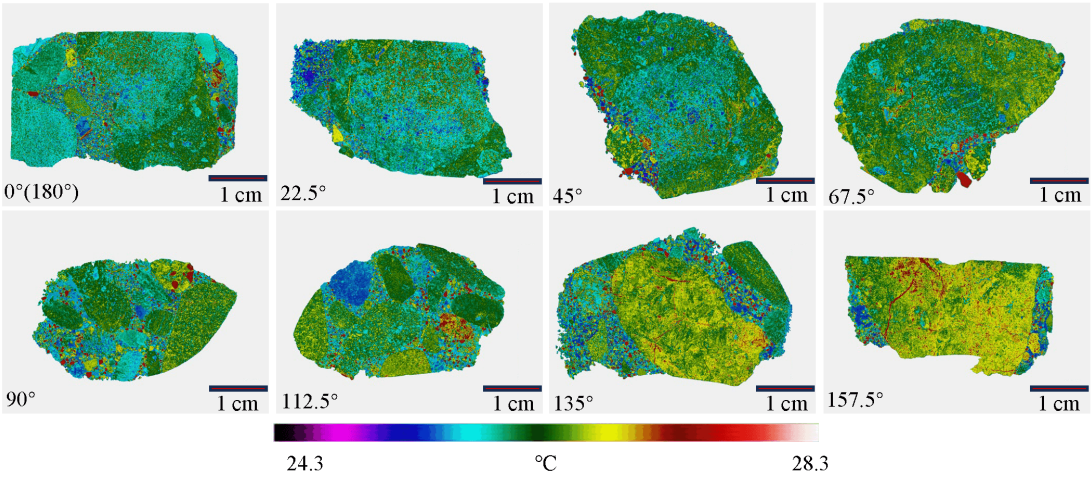

Fig. 7. Full-field apparent temperature distribution images of eight-directional slices of tight conglomerates.

Table 1. Apparent temperature value corresponding to various reservoir components (°C).

Mineral	Color	Maximum	Minimum	Average
Quartz	Red	27.53	27.22	27.49
Weakly weathered feldspar	Yellow	26.97	26.68	26.85
Moderately weathered feldspar	Green	26.27	26.01	26.16
Strongly weathered feldspar	Cyan	25.99	25.72	25.82
Clay minerals	Blue, light purple	25.60	25.42	25.49

3.3.2 Component characterization

To enhance conclusion representativeness and balance resolution with observation scale, a macro-lens infrared thermal imager was coupled with a displacement stage and large-field image stitching technology to acquire full-field apparent temperature distribution maps of the 8 directional slices. Fig. 7 presents these maps. All slices are predominantly composed of five characteristic minerals: Quartz marked in red, strongly weathered feldspar in cyan, moderately weathered feldspar in green, weakly weathered feldspar in yellow, and clay minerals in blue-purple. No new mineral types are added or existing ones lost across directions. This compositional consistency forms the reservoir rock's basic mineral framework, indicating macro-scale homogeneity in the core sample's mineral composition.

Quartz exists as isolated single particles or small double-particle aggregates in all slices, with uniformly subangular-subrounded shapes embedded in feldspar gaps. Light halos at some quartz edges indicate intergranular micropores, and existing unfilled linear microfractures show no directional bias, reflecting quartz's strong resistance to diagenetic alteration. Strongly weathered feldspar appears as continuous blocks or irregular flakes and serves as the matrix mainstay, with jagged mineral contacts, widespread honeycomb micropores, and local clay impregnation. It shows a gradual transition with moderately weathered feldspar and no abrupt interfaces, which highlights the continuity of feldspar weathering. Moderately weathered feldspar has semi-angular boundaries and discontinuous serrated dissolution notches, often forming a "yellow core-green ring" coating or transition structure with weakly weathered feldspar, confirming a progressive weathering sequence unchanged by slice direction. Weakly weathered feldspar occurs as intact ellipsoids or short columns without obvious dissolution, mostly within or at the edges of moderately weathered feldspar, and some preserve original crystalline bedding, which indicates minimal diagenetic impact. Clay minerals distribute as fine dots or branched microveins, showing selective occurrence that mainly includes particle edge coatings or incomplete pore and fracture filling, without macro-scale directional enrichment, confirming a stable "dispersion-selective filling" pattern.

Beyond this macro homogeneity, component heterogeneity and anisotropy stand out in three interrelated aspects. First, mineral volume fractions exhibit directional fluctuations. Quartz volume fraction varies slightly between 4% and 6% with no obvious directional trend, reflecting local micro-area differences. Strongly weathered feldspar decreases significantly, with accelerated decline in certain directional ranges, indicating directional distribution differences. Moderately weathered feldspar fluctuates between 25%-38%, peaking in one direction and troughing in another, and shows a negative correlation to strongly weathered feldspar that reflects a weathering degree trade-off. Weakly weathered feldspar increases directionally, accelerating in certain directional ranges, confirming a directional enrichment zone and showing a

Table 2. Full-field component content of 8-directional slices of tight conglomerate (%).

Direction	Quartz	Strongly weathered feldspar	Moderately weathered feldspar	Weakly weathered feldspar	Clay minerals
0° (180°)	4	55	32	6	3
22.5°	5	45	35	7	8
45°	6	40	35	8	11
67.5°	4	42	38	7	9
90°	5	38	35	10	12
112.5°	6	35	30	12	17
135°	4	32	28	25	11
157.5°	5	30	25	32	8

strict negative correlation to strongly weathered feldspar. Clay minerals fluctuate between 3%-17%, peaking in one direction, and correlate positively with feldspar weathering intensity. Second, mineral spatial distribution shows directional differences. Quartz is scattered in some slices but locally enriched in others. Strongly weathered feldspar occupies the matrix core in some slices but retreats to edge or transition zones in others. Weakly weathered feldspar shifts from scattered in some slices to core enrichment in others. Third, microstructure and diagenetic responses vary directionally. Quartz shows slightly higher roundness only in some slices, implying longer transport distance. Strongly weathered feldspar has lower honeycomb micropore density and a clearer transition zone in some slices, while transition zone alteration reflects diagenetic gradualism in others. Moderately weathered feldspar has longer band extension and shallower dissolution notches in some slices, and occurs as large blocks in some directions while being patchy or banded in others. Weakly weathered feldspar has higher density and clearer crystalline bedding in some slices, and forms aggregates in some directions while remaining isolated in others. Clay minerals have more microveins, thicker coatings, and higher incomplete filling ratios in some slices, show directional microvein extension in certain directional ranges, and have large-block distribution in others. These trends are further validated by component content tests, as shown in Table 2, which confirm the directional variations in each mineral's proportion.

Geologically, quartz's uniform distribution reflects homogeneous transport and deposition during sedimentation-diagenesis. Directional differences in feldspar weathering, which manifest as decreasing strong weathering and increasing weak weathering, reveal diagenetic anisotropy such as fluid dissolution and metasomatism, linked to paleofluid migration direction or original rock fabric. The positive correlation between clay minerals and feldspar weathering confirms feldspar weathering as a key clay source, and diagenetic environment directionality, including variations in fluid chemistry and migration channels, controls clayization intensity. Engineering-wise, weakly weathered feldspar-enriched zones have intact mineral structures that favor high-quality reservoir space, enhancing porosity and permeability. Clay-rich zones pose reservoir damage risks due to clay water sensitivity such as swelling and pore blocking, requiring targeted prevention in drilling and fracturing. The directional distribution of feldspar weathering underscores anisotropic reservoir heterogeneity, which must be considered in reservoir evaluation and development design, such as horizontal well trajectory optimization, to improve efficiency.

Overall, the 8 directional slices demonstrate the tight conglomerate's macro stability in mineral composition and occurrence, alongside the continuity of its mineral framework and diagenesis. The directional fluctuations in mineral content, spatial distribution, and microstructure provide direct microscopic insights for subsequent reservoir heterogeneity evaluation and directional diagenetic research. These fluctuations are manifested in weakly weathered feldspar's "scattered-to-enriched" shift and clay enrichment alongside stronger feldspar weathering.

3.4 Mechanisms and implications

Plots reveal the coupling between infrared apparent temperature and elemental distribution. Oxygen and potassium contents increase with the maximum apparent temperature, as shown in Figs. 8(a) and 8(b) respectively. This aligns with the thermal radiation characteristics of rock-forming minerals like quartz and K-feldspar. In contrast, sodium contents decrease linearly with both maximum and average apparent temperatures, as shown in Figs. 8(c) and 8(d) respectively. This reflects sodium leaching during diagenetic alteration such as plagioclase dissolution. These correlations bridge thermal infrared responses with geochemical features, enabling rapid characterization of elemental and mineral variations in tight conglomerates via infrared imaging and clarifying the diagenetic control on thermal properties-element migration coupling. Fig. 8 shows correlations between apparent infrared temperature and element contents. Furthermore, additional analyses of coupling relationships among pores, elements, and mineral components reveal generally low correlation coefficients. Most R^2 values are less than 0.5, failing to meet the traditional criterion for statistically significant correlation. This weak correlation directly reflects the geological complexity of the study

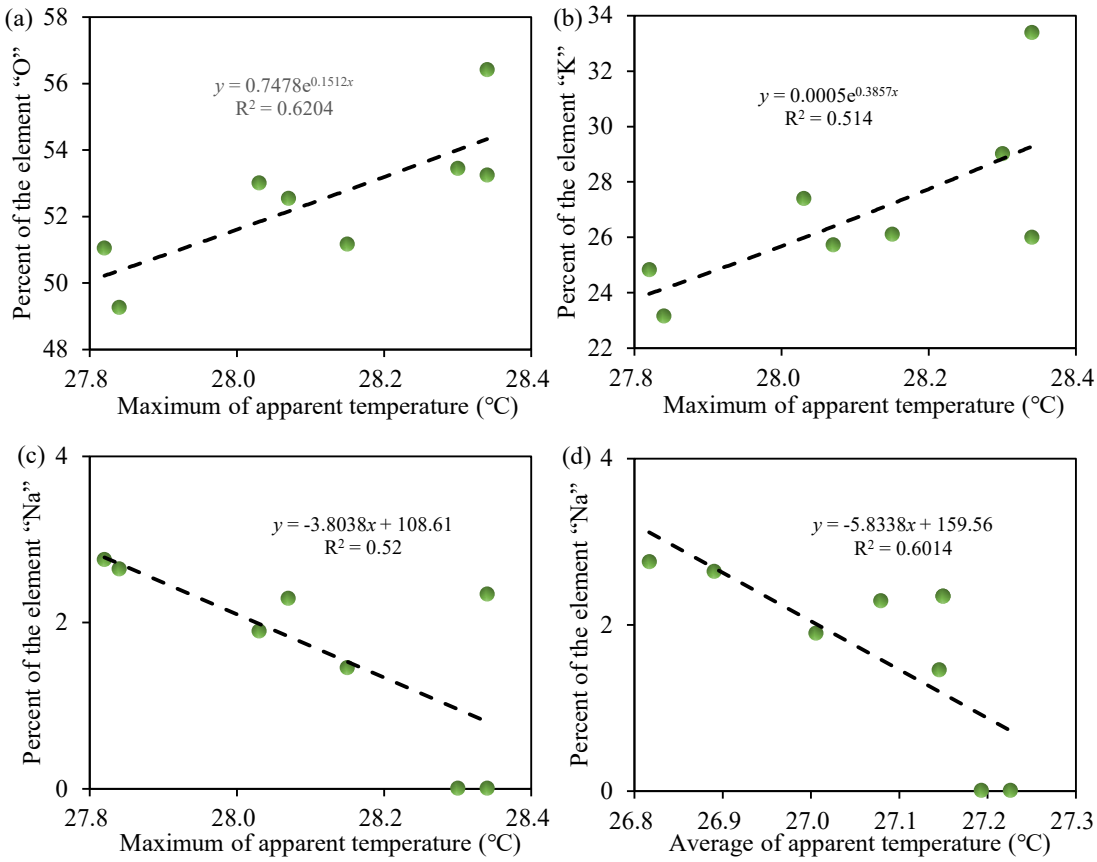

Fig. 8. Correlations between apparent infrared temperature and element contents: (a) indicates O content vs. maximum temperature, (b) shows K content vs. maximum temperature, (c) points to Na content vs. maximum temperature and (d) indicates Na content vs. average temperature.

area's tight conglomerate reservoirs. The tight conglomerates have undergone multi-stage diagenetic modifications, characterized by the superposition of compaction, cementation, and dissolution processes. Moreover, fluid activity intensity and mineral transformation pathways vary across different directions. Consequently, pore development is not only controlled by the weathering of individual minerals but also influenced by multiple factors, including gravel arrangement and late-stage cement filling. These non-ideal quantitative results are not meaningless. Instead, they uncover the intrinsic nature of tight conglomerate reservoir microscopic features being controlled by the coupling of multiple mechanisms – a typical characteristic distinguishing unconventional reservoirs from conventional ones. Furthermore, this finding provides critical insights for subsequent in-depth analysis of the cascading effects of sedimentation-diagenesis-microscopic characteristics. Thus, although no strong correlation is observed between the aforementioned parameters, the quantitative analysis process itself confirms the complexity of the reservoir's microscopic features. This aligns with the core objective of the present study – establishing a multi-technique integrated characterization system – and also offers a reference perspective for research on similar complex reservoirs.

In this research, pore, element, and component heterogeneity and anisotropy in the tight conglomerate reservoir are all distinctly pronounced. In the pore dimension, the maximum/minimum mean value ratio for all size parameters (such as radius, Feret diameter) and morphological parameters (such as aspect ratio, boundary shape factor) exceeds 1. For instance, the aspect ratio exhibits a Max/Min mean ratio of 1.13, confirming directional differences in pore geometry. In the element dimension, characteristic elements like Na, K, and Fe show clear directional enrichment and depletion. K content reaches high levels in one direction, while Na content is extremely low in another, reflecting geochemical fractionation driven by fluid activity. In the component dimension, mineral relative contents (such as weakly weathered feldspar showing an increasing trend across directions) and spatial distributions (such as strongly weathered feldspar migrating from the matrix core to edge zones with directional changes) display obvious angle dependence. Collectively, these observations confirm that the reservoir has no absolute homogeneity, with differences manifesting progressively across micro-scales (namely pores), geochemical scales (namely elements), and mineralogical scales (namely components).

Fundamentally, all three types of heterogeneity and anisotropy are synergistically controlled by the original sedimentary fabric and late diagenesis. The orientation of gravel arrangement in the original fabric defines the dominant channels for fluid migration, which in turn imparts directionality to

diagenetic processes. For pores, fabric orientation drives the development of dissolution pores along dominant directions, resulting in larger pore sizes in certain directions. For elements, fluid migration along these channels causes leaching of soluble components like Na and Mg, leading to their depletion in some directions and enrichment of insoluble or secondary components like K and Fe in others. For components, directional variations in fluid activity intensity lead to differences in feldspar weathering degrees and directional occurrence of clay minerals. Importantly, these three sets of characteristics also provide a microscopic scientific basis for reservoir development design. Pore-dominant seepage directions, fluid channels indicated by element depletion (such as Na-depleted zones), weakly weathered feldspar-enriched zones, and clay-sensitive zones mutually corroborate each other, collectively pointing to the engineering strategy of prioritizing wellbore deployment in pore-dominant seepage directions and weakly weathered feldspar-enriched zones while avoiding fracturing in clay-enriched zones.

Mechanistically, tight interconnections exist between the three types of heterogeneity and anisotropy. First, mineral type and weathering state in the component dimension directly determine pore development potential. Strongly weathered feldspar, a component, forms honeycomb-like micropores due to crystal structure damage, and its directional distribution shapes the spatial pattern of high-value pore zones. Concurrently, mineral composition (such as Si in quartz and Na/K in feldspar) provides material sources for elements. Na and K released by feldspar weathering migrate through pore channels, leading to directional element enrichment and depletion. This forms a chain effect where component (mineral) leads to pore (channel) and then element migration. Second, the dominant development directions of pores act as main channels for fluid migration, directly controlling the spatial pattern of element fractionation. For example, one direction is not only a high-value zone for pore radius but also a depletion zone for Na and Mg, confirming that fluids intensify leaching of soluble components through dominant pore channels. Meanwhile, chemical substances like Ca^{2+} and Si^{4+} carried by pore fluids can undergo cementation, forming calcite or siliceous cement. This in turn alters pore morphology (such as increased boundary shape factor values and smoother boundaries) and component composition (with cements becoming new components), reflecting a feedback mechanism where pore (channel) leads to element (cementation) and then pore-component transformation. Third, element ratios quantify the diagenetic intensity of the pore-component system. A high Si/Al ratio in one direction corresponds to relative quartz enrichment and intense feldspar weathering, indirectly indicating more developed pores in this zone via feldspar dissolution. Differences in K/Na ratios, with extremely high values in one direction and values less than 1 in another, reveal the directionality of potassium metasomatism. High ratios overlap weakly weathered feldspar-enriched zones, confirming that K-bearing fluids do not significantly damage feldspar structures, thereby preserving intact mineral particles and high-quality pores. This enables reverse tracing from element ratio to component weathering and then to pore quality.

Finally, pore, element, and component heterogeneity and anisotropy are differential manifestations of the same geological process, which encompasses sedimentation and diagenesis, across distinct dimensions. Components serve as the material basis, pores as the spatial carriers, and elements as the chemical response. The three are coupled through the chain process of mineral weathering, then pore development, then fluid migration, and finally element differentiation, collectively determining the reservoir's macroscopic physical properties and development potential. Their synergistic analysis provides a multi-dimensional microscopic foundation for refined reservoir evaluation and optimization of development schemes.

3.5 Limitations and prospects

An integrated micro-characterization framework for tight conglomerate reservoirs has been established, yet several limitations should be acknowledged. The current interpretations regarding sedimentary fabric controls on fluid flow and paleo-fluid migration directions would benefit from more direct evidence. Specifically, systematic gravel orientation statistics and geochemical data from fluid inclusions or stable isotopes are not yet available. Moreover, establishing fully quantitative relationships between mineral alteration intensity and pore development requires further investigation.

Future work will focus on acquiring these critical datasets through detailed fabric analysis and geochemical characterization. Integrating three-dimensional techniques like micro-CT is essential to validate the three-dimensional structures inferred from two-dimensional anisotropy measurements. This validation will establish predictive models that reliably connect microscopic heterogeneity with macroscopic reservoir performance.

4. Conclusions

This study takes the tight conglomerate reservoir as the core research object. By coupling macro-lens infrared thermal imaging with the "umbrella deconstruction" method and SEM/EDS, this study establishes an integrated technical system. It systematically reveals the heterogeneity and anisotropy of reservoir pores, elements, and components, providing microscopic theoretical support for the efficient development of this type of reservoir.

1) An integrated technical system for characterizing the heterogeneity and anisotropy of tight conglomerates is constructed. Macro-lens infrared thermal imaging can realize second-level thermal signal acquisition. It allows dynamic observation without sample coating treatment, effectively making up for the limitations of traditional scanning electron microscopy and energy dispersive spectroscopy, such as low batch processing efficiency and inability to perform dynamic monitoring.
2) The pores, elements, and components of the tight conglomerate reservoir all show significant heterogeneity and anisotropy: Pores are more developed in some specific directions; elements exhibit directional enrichment and depletion. The proportion of weakly weathered feldspar increases from 6% to 32% with increasing angle.

3) The multi-dimensional heterogeneity and anisotropy of the reservoir are synergistically controlled by the original sedimentary fabric and late diagenesis. The original gravel arrangement determines the dominant channels for fluid migration, thereby affecting the directionality of diagenetic processes such as dissolution and leaching, leading to angle-dependent differences in reservoir characteristics.
4) The research findings can provide clear guidance for reservoir development scheme design. In engineering, priority can be given to selecting pore seepage-dominant directions and weakly weathered feldspar-enriched areas for wellbore deployment, while avoiding fracturing in clay mineral-enriched areas. This aims to reduce reservoir damage and improve development efficiency.

Acknowledgements

This work was jointly supported by National Natural Science Foundation of China (No. 12241205), Beijing Natural Science Foundation (No. 8232054), Young Elite Scientists Sponsorship Program by BAST (No. BYESS2023182), and Oil & Gas Major Project (No. 2025ZD1405006).

Conflict of interest

The authors declare no competing interest.

References

Abitkazy, T., He, Y., Chen, F., et al. Research on the influence of mineral heterogeneity under different CO_2 injection schemes in low permeability reservoirs. Natural Gas Industry B, 2024, 11(3): 291-302.

Balatsenko, O. N. Environmentally stabilized thermal-imaging optical systems. Journal of Optical Technology, 2023, 90(9): 491-497.

Camp, W. K., Lewan, M. D., Floyd, M., et al. Scanning electron microscopy of tight oil reservoirs before and after low-temperature hydrous pyrolysis, lower Permian Wolfcamp shale, Delaware Basin, Texas. AAPG Bulletin, 2025, 109(3): 335-364.

Cha, D. H., Kim, H. J., Hwang, Y., et al. Fabrication of molded chalcogenide-glass lens for thermal imaging applications. Applied Optics, 2012, 51(23): 5649-5656.

Chen, D., Zhong, H., Wang, Z., et al. Modelling spontaneous droplet transport in deformable divergent channels. Capillarity, 2025, 15(1): 4-11.

Du, S. Profound connotations of parameters on the geometric anisotropy of pores in which oil store and flow: A new detailed case study which aimed to dissect, conclude and improve the theoretical meaning and practicability of "Umbrella Deconstruction" method furtherly. Energy, 2020, 211: 118630.

Du, S., Bai, L., Zhao, A., et al. Infrared thermal imaging under a macro lens empowers geo-energy exploration and development: Application scenarios and scheme conceptions. Advances in Geo-Energy Research, 2025, 16(1): 4-7.

Du, S., Pang, S., Shi, Y. Quantitative characterization on the microscopic pore heterogeneity of tight oil sandstone reservoir by considering both the resolution and representativeness. Journal of Petroleum Science and Engineering, 2018, 169: 388-392.

Du, S., Xu, F., Taskyn, A., et al. Anisotropy characteristics of element composition in Upper Triassic "Chang 8" shale in Jiyuan district of Ordos Basin, China: Microscopic evidence for the existence of predominant fracture zone. Fuel, 2019, 253: 685-690.

Eaton, T. T. On the importance of geological heterogeneity for flow simulation. Sedimentary Geology, 2006, 184(3-4): 187-201.

Fjær E., Nes, O. M. The impact of heterogeneity on the anisotropic strength of an outcrop shale. Rock mechanics and Rock Engineering, 2014, 47(5): 1603-1611.

Fitch, P. J. R., Lovell, M. A., Davies, S. J., et al. An integrated and quantitative approach to petrophysical heterogeneity. Marine and Petroleum Geology, 2015, 63: 82-96.

Guo, J., McCaffrey, K., Jones, R., et al. The spatial heterogeneity of structures in high porosity sandstones: Variations and granularity effects in orientation data. Journal of Structural Geology, 2009, 31(7): 628-636.

Hou, F., Zhang, Y., Zhou, Y., et al. Review on infrared imaging technology. Sustainability, 2022, 14(18): 11161.

Kazak, A., Simonov, K., Kulikov, V. Machine-learning-assisted segmentation of focused ion beam-scanning electron microscopy images with artifacts for improved void-space characterization of tight reservoir rocks. SPE Journal, 2021, 26(4): 1739-1758.

Khanal, S., Fulton, J., Shearer, S. An overview of current and potential applications of thermal remote sensing in precision agriculture. Computers and Electronics in Agriculture, 2017, 139: 22-32.

Khattak, S. A., Hanif, M., Ahmad, S., et al. Sedimentology and reservoir characterization of Upper Cretaceous Kawagarh Formation, Upper Indus Basin, Lesser Himalayas, Pakistan: Inferences from petrography, SEM-EDS and petrophysics. Carbonates and Evaporites, 2024, 39(3): 72.

Liu, J., Zhang, D., Liu, S., et al. Multiscale investigation into EOR mechanisms and influencing factors for CO_2-WAG injection in heterogeneous sandy conglomerate reservoirs using NMR technology. Petroleum Science, 2025, 22(7): 2977-2991.

Liu, Y., Liu, A., Liu, S., et al. Nano-scale mechanical properties of constituent minerals in shales investigated by combined nanoindentation statistical analyses and SEM-EDS-XRD techniques. International Journal of Rock Mechanics and Mining Sciences, 2022, 159: 105187.

Mokhtari, M., Honarpour, M. M., Tutuncu, A. N., et al. Characterization of elastic anisotropy in Eagle Ford Shale: Impact of heterogeneity and measurement scale. SPE Reservoir Evaluation & Engineering, 2016, 19(03): 429-439.

Molineux, J., Lee, T., Kim, K. J., et al. Fabrication of plastic optics from chalcogenide hybrid inorganic/organic polymers for infrared thermal imaging. Advanced Optical Materials, 2024, 12(7): 2301971.

Qin, X., Wang, H., Xia, Y., et al. Three-dimensional modeling of nanoconfined multiphase flow in clay nanopores using FIB-SEM images of shale. The Innovation Energy, 2024, 1(4): 100050.

Sinan, S., Glove, P. W. J., Lorinczi, P. Modelling the impact of anisotropy on hydrocarbon production in heterogeneous reservoirs. Transport in Porous Media, 2020, 133(3): 413-436.

Sun, J., You, X., Zhang, Q., et al. Development characteristics and genesis of deep tight conglomerate reservoirs of Mahu area in Junggar Basin, China. Journal of Natural Gas Geoscience, 2023, 8(3): 201-212.

Sun, Y., Zhao, Y., Yuan, L. Quantifying nano-pore heterogeneity and anisotropy in gas shale by synchrotron radiation nano-CT. Microporous and Mesoporous Materials, 2018, 258: 8-16.

Tan, C., Yu, X., Liu, B., et al. Conglomerate categories in coarse-grained deltas and their controls on hydrocarbon reservoir distribution: A case study of the Triassic Baikouquan Formation, Mahu Depression, NW China. Petroleum Geoscience, 2017, 23(4): 403-414.

Tan, F., Li, X., Ma, C., et al. Genetic mechanism of permeability anisotropy in conglomerate reservoir and its controlling factors. Geological Society of America Bulletin, 2023, 135(3-4): 852-866.

Wang, J., Yang, C., Liu, Y., et al. Creep behavior of marine Wufeng-Longmaxi Formation shales in the Sichuan Basin, Southwest China characterized at micro scale: A case study of exploration well SQ-1 in Sanquan Town, Nanchuan District, Chongqing. Natural Gas Industry B, 2024a, 11(4): 357-367.

Wang, X., Meng, S., Ostadhassan, M., et al. Detecting shale oil hidden in nanopores using a novel electron microscopy method. The Innovation Energy, 2024b, 1(1): 100011.

Wang, Z., Ge, H., Zhou, W., et al. Characterization of pores and microfractures in tight conglomerate reservoirs. International Journal of Hydrogen Energy, 2022, 47(63): 26901-26914.

Wood, D. A. Expanding role of borehole image logs in reservoir fracture and heterogeneity characterization: A review. Advances in Geo-Energy Research, 2024, 12(3): 194-204.

Worden, R. H., Utley, J. E. P. Automated mineralogy (SEM-EDS) approach to sandstone reservoir quality and diagenesis. Frontiers in Earth Science, 2022, 10: 794266.

Yu, Z., Wang, Z., Jiang, Q., et al. Evaluation of low permeability conglomerate reservoirs based on petrophysical facies: A case study from the Triassic Baikouquan Formation, northern Mahu Sag, Junggar Basin, China. Journal of Petroleum Science and Engineering, 2022, 219: 111082.

Zhai, T., Zhao, Z., Zhou, X. A review of 3D reconstruction methods for complex microstructures of porous media: Imaging devices, techniques and applications. Rock Mechanics and Rock Engineering, 2025, 58(7): 7879-7922.

Zhang, S., Liu, Y., Li S., et al. Method for constructing a reservoir architectural parameter database based on literature data collection and its practical application: A case study of braided river reservoirs. Petroleum Science Bulletin, 2024, 9(6): 885-898. (in Chinese)

Zhang, Z., Qin, Y., Zhuang, X., et al. Poroperm characteristics of high-rank coals from Southern Qinshui Basin by mercury intrusion, SEM-EDS, nuclear magnetic resonance and relative permeability analysis. Journal of Natural Gas Science and Engineering, 2018, 51: 116-128.

Zhan, H., Yang, Q., Qin, F., et al. Comprehensive preparation and multiscale characterization of kerogen in oil shale. Energy, 2022, 252: 124005.

Zhao, A., Du, S. Hydration-induced damage of tight conglomerates. Chemical Engineering Journal, 2024, 495: 153426.

Zimmermann, U., Madland, M. V., Nermoen, A., et al. Evaluation of the compositional changes during flooding of reactive fluids using scanning electron microscopy, nano-secondary ion mass spectrometry, X-ray diffraction, and whole-rock geochemistry. AAPG Bulletin, 2015, 99(5): 791-805.

Zoccarato, C., Bau, D., Bottazzi, F., et al. On the importance of the heterogeneity assumption in the characterization of reservoir geomechanical properties. Geophysical Journal International, 2016, 207(1): 47-58.